This is the Author Accepted Manuscript.

There may be differences between this version and the published version. You are advised to consult the publisher's version if you wish to cite from it.

https://eprints.gla.ac.uk/225752/

Deposited on: 29 October 2020

The lid domain is important, but not essential, for catalysis of *Escherichia coli* pyruvate kinase

Elena Sugrue[1, 2 #], David Coombes[1, #], David Wood[1], Tong Zhu[1], Katherine A Donovan[1, 3, 4] & Renwick C.J. Dobson[1, 5, *]

[1]Biomolecular Interaction Centre and School of Biological Sciences, University of Canterbury, PO Box 4800, Christchurch 8140, New Zealand

[2]MRC-University of Glasgow Centre for Virus Research, Glasgow G61 1QH, United Kingdom

[3]Department of Cancer Biology, Dana–Farber Cancer Institute, Boston, Massachusetts 02215, USA

[4]Department of Biological Chemistry and Molecular Pharmacology, Harvard Medical School, Boston, Massachusetts 02115, USA

[5]Biol21 Molecular Science and Biotechnology Institute, Department of Biochemistry and Molecular Biology, University of Melbourne, Parkville, Victoria 3010, Australia

[#] These authors contributed equally to this work

[*] Corresponding author: Renwick C. J. Dobson, renwick.dobson@canterbury.ac.nz

ORCID:

Elena Sugrue: 0000-0001-5014-9522

David Coombes: 0000-0001-6384-2617

David Wood: 0000-0002-8275-3510

Katherine A Donovan: 0000-0002-8539-5106

Renwick C.J. Dobson: 0000-0002-5506-4939

Abstract

Pyruvate kinase catalyses the final step of the glycolytic pathway in central energy metabolism. The monomeric structure comprises three domains: a catalytic TIM-barrel, a regulatory domain involved in allosteric activation, and a lid domain that encloses the substrates. The lid domain is thought to close over the TIM-barrel domain forming contacts with the substrates to promote catalysis and may be involved in stabilising the activated state when the allosteric activator is bound. However, it remains unknown whether the lid domain is essential for pyruvate kinase catalytic or regulatory function. To address this, we removed the lid domain of *Escherichia coli* pyruvate kinase type 1 (PK$^{TIM+Reg}$) using protein engineering. Biochemical analyses demonstrate that, despite the absence of key catalytic residues in the lid domain, PK$^{TIM+Reg}$ retains a low-level of catalytic activity and has a reduced binding affinity for the substrate phosphoenolpyruvate. The enzyme retains allosteric activation, but the regulatory profile of the enzyme is changed relative to the wild-type enzyme. Analytical ultracentrifugation and small-angle X-ray scattering data show that, beyond the loss of the lid domain, the PK$^{TIM+Reg}$ structure is not significantly altered and is consistent with the wild type tetramer that is assembled through interactions at the TIM and regulatory domains. Our results highlight the contribution of the lid domain for facilitating pyruvate kinase catalysis and regulation, which could aid in the development of small molecule inhibitors for pyruvate kinase and related lid-regulated enzymes.

(234 words)

Introduction

Glycolysis is the central energy-generating pathway in most organisms (Van Schaftingen 1993). The pathway catalyses the breakdown of glucose into pyruvate and this is coupled to energy generation *via* the synthesis of reduced nicotinamide adenine dinucleotide (NADH) and adenosine triphosphate (ATP) that are then used to drive further biosynthetic processes (Ainscow and Brand 1999; Xie and Wang 1996). The final step of glycolysis is catalysed by the enzyme pyruvate kinase and this reaction is often allosterically regulated by one or more effectors.

In *Escherichia coli*, the pyruvate kinase type 1 monomer consists of three domains (Zhu et al. 2010). The catalytic domain (residues 1–70, 171–351) is a typical TIM barrel (also known as a $(\beta/\alpha)_8$-barrel), a common structural fold found in a diverse selection of enzymes that has a variety of functions (Sterner and Höcker 2005). The catalytic domain contains many of the active site residues needed for binding the substrates (phosphoenolpyruvate and adenosine diphosphate), as well as binding cations (K^+, Mg^{2+}) that interact with the substrates and are essential for catalysis (Mattevi et al. 1995). The lid domain (residues 71–170) folds over the active site of the catalytic domain and consists of a small intertwined β-barrel assembly (Mattevi et al. 1995). Finally, the C-terminal regulatory domain (residues 352–470) binds the allosteric activator, fructose-1,6-bisphosphate, which induces a conformational shift to the active R-state (Mattevi et al. 1995). In solution, *E. coli* pyruvate kinase forms a stable tetramer (Zhu et al. 2010), which enables co-operative activation between monomers upon the binding of the substrate phosphoenolpyruvate (Valentini et al. 2000). The tetramer is formed through two interfaces, the first between the catalytic domains forming a dimer, and the second interface lies between the regulatory domains to form a dimer of dimers (PDB: 4YNG) (Donovan et al. 2016b; Mattevi et al. 1995). The face-to-face assembly forms an oblate structure with a hole in the centre that resembles a ring doughnut from a side on view.

As a central metabolic pathway, glycolysis is highly regulated. This includes allosteric regulation by phosphofructokinase in the early stage of the pathway, and by pyruvate kinase in the final step (Fenton and Reinhart 2002; Reeves and Sols 1973; Valentini et al. 2000). Although the allosteric modulator varies between species, in *E. coli*, pyruvate kinase type 1 is regulated through two activators: fructose-1,6-bisphosphate, an early pathway substrate of glycolysis that binds allosterically at the regulatory domain; and phosphoenolpyruvate, the enzyme substrate, which

cooperatively binds at the active site (Mattevi et al. 1995). Activation of pyruvate kinase plays a role in increasing flux through the glycolytic pathway (Mattevi et al. 1995; Pearce et al. 2001). The mechanism of allosteric activation of *E. coli* pyruvate kinase type 1 is thought to occur *via* conformational changes upon binding fructose-1,6-bisphosphate and has been discussed in detail elsewhere (Mattevi et al. 1996; Schormann et al. 2019). Briefly, binding of fructose-1,6-bisphosphate stabilises a 20-40° rotation at the regulatory domain (Schormann et al. 2019; Valentini et al. 2000), which increases dynamic movement in the TIM domain around the active site (Donovan et al. 2016b), and places the lid domain near the opposing monomer, increasing interaction to close the lid (Mattevi et al. 1995).

One aspect of the pyruvate kinase enzyme that has not been extensively investigated is the function of the lid domain. The domain is a distinct β-barrel fold with six anti-parallel beta strands that belongs to the pyruvate kinase β-barrel domain family (SCOP ID: 4002474). The domain is well-conserved, appearing in all three phylogenetic domains of life, with a high degree of similarity between evolutionary distinct organisms (Johnsen et al. 2003; Pendergrass et al. 2006; Schormann et al. 2019). This suggests that the lid domain of pyruvate kinase is likely to be both ancient and important. The domain has been documented to be highly mobile, a characteristic that underpins its expected function within catalysis and regulation. It is proposed that after metal cations coordinate in the active site, the lid domain rotates to allow substrate binding, after which it moves to cover and dehydrate the active site cleft (Li et al. 2012; Naithani et al. 2015). The position and amount of movement seen in the lid is known to vary depending upon substrate binding within the active site and whether fructose-1,6-phosphate is bound at the regulatory domain (Li et al. 2012; Valentini et al. 2000). However, experiments that have provided these insights are generally focused on catalysis (Oria-Hernández et al. 2005), regulation (Valentini et al. 2000), or deficiencies in human pyruvate kinase mutants (Valentini et al. 2002; van Wijk et al. 2009), and only involve site directed mutagenesis studies. As such, implications for the ubiquitous and structurally distinctive lid domain have not been reported. Therefore, it remains unknown whether the lid domain is essential for pyruvate kinase catalytic or regulatory function.

Thus, to determine whether the lid domain is essential for catalytic and regulatory function of *E. coli* pyruvate kinase type 1, we removed this domain from the protein to create a pruned enzyme consisting of the catalytic TIM barrel and regulatory domains (PK$^{TIM+Reg}$). We found that the PK$^{TIM+Reg}$ enzyme binds the substrates phosphoenolpyruvate and adenosine diphosphate and is

catalytically active, but that enzyme activity is severely attenuated. Thermal stability assays show that the activator, fructose-1,6-bisphosphate, still binds to $PK^{TIM+Reg}$, while solution studies show that the cleaved enzyme retains its doughnut-shaped tetramer assembly, similar to the wild-type structure. These data show that the lid domain is not essential for structural formation or enzyme function, but it is necessary for the high-levels of catalytic turnover that are expected for a glycolytic enzyme.

Materials and methods

Cloning, expression and purification

A truncated pyruvate kinase enzyme was generated using a nucleotide sequence synthesised by Genscript (Korea). The PK$^{TIM+Reg}$ construct consisted of sequence corresponding to aa 1–70 and 171–470 (catalytic and regulatory domains) of wild-type pyruvate kinase from *E. coli* strain REL606 (Accession number: AY849930.1), with a proline to alanine substitution at residue 70 (P70A). The construct was ligated into expression vector pET-26b+ using the NdeI and BamHI restrictions sites to add a thrombin cleavage site and a 6×-histidine tag to the C-terminal end of the construct. The resulting vector was then transformed into chemically-competent *E. coli* BL21(DE3) cells.

Protein expression and purification were carried out as described previously for the wild-type enzyme (Donovan et al. 2016a). Briefly, recombinant *E. coli* containing the mutant construct were cultured at 37 °C in 1 L of Luria-Bertani broth supplemented with 30 mg of kanamycin to an optical density at 600 nm of 0.6. Expression was induced by the addition of 1 mM isopropyl β-d-1-thiogalactopyranoside and the culture was incubated at 26 °C overnight. Cells were collected by centrifugation at 10,000 × *g* for 10 min in a Thermo Sorvall RC-6-Plus centrifuge and the supernatant was discarded. The collected cells were then resuspended in Buffer A (20 mM Tris-HCl, 500 mM NaCl, 20 mM imidazole, pH 8) and lysed using a Hielscher UP200S Ultrasonic Homogenizer at 70% with a 0.5 s on/off cycle for 7 min. The lysate was centrifuged at 10,000 × *g* for 40 min in an Eppendorf 5810R centrifuge and the supernatant recovered before being applied to a GE Healthcare HisTrap FF Crude 5-mL column pre-equilibrated with five column volumes of Buffer A. A gradient (0%–100%) of Buffer B (20 mM Tris-HCl, 500 mM NaCl, 500 mM imidazole, pH 8) was then applied over 18 column volumes. Peak fractions were determined based on the ultraviolet (UV) intensity at 280 nm and sodium dodecyl sulphate polyacrylamide gel electrophoresis (SDS-PAGE) analysis. The fractions were then applied to a HiLoad 16/60 Superdex column pre-equilibrated with Buffer C (20 mM Tris-HCl, 150 mM NaCl, pH 8). Peak fractions were again determined by 280 nm UV intensity and SDS-PAGE analyses. Fractions were then pooled, flash-frozen and stored at −80 °C. Steps performed at 4°C, except when noted otherwise.

Kinetic assays

The kinetic parameters of the PK$^{TIM+Reg}$ enzyme were determined using a lactate dehydrogenase coupled assay, as described previously (Malcovati and Valentini 1982). Initial rates were

determined from the decrease in NADH concentration, as measured at 340 nm using a CARY 100 Bio UV-Visible spectrophotometer (Agilent Technologies). The 1-mL reaction volumes contained 10 mM HEPES (pH 7.5), 50 mM KCl, 10 mM $MgCl_2$, 2 mM fructose-1,6-bisphosphate, 120 µM NADH, 22 units of lactate dehydrogenase (Sigma-Aldrich) and 280 nM purified PK[TIM+Reg]. When varying the concentration of either adenosine diphosphate or phosphoenolpyruvate, the other substrate was kept at 2 mM. Curve fitting for kinetic parameters was performed in Origin (OriginPro, version 8.5).

Differential scanning fluorimetry

Differential scanning fluorimetry was performed using the BioRad IQ5 Multicolor RealTime PCR Detection System based on a previously described method (Niesen et al. 2007). Briefly, protein (50 µL, 1 mg/mL), SYPRO orange dye (1 µL) (Thermo Fisher Scientific) and varying concentrations of ligand were added to the wells of a 96-well plate. Each reaction was made up to a final volume of 100 µL with a buffer consisting of 20 mM Tris-HCl and 150 mM NaCl, pH 8. The reaction temperature was increased from 20 °C to 100 °C in 1 °C increments, with each temperature held for 20 s prior to measuring. The unfolding temperature was determined by the dRFU/dt.

Homology model building and molecular dynamic simulation

An atomic model of the PK[TIM+Reg] mutant protein was constructed using SWISS-MODEL (Arnold et al. 2006) with *E. coli* pyruvate kinase (PDB: 4YNG) as a template. Additional residues in the polyhistidine region were manually built using the COOT model software package (Emsley et al. 2010). Molecular dynamics simulations were conducted with Gromacs (version 5.0.6) (Abraham et al. 2015) using a simplified protocol based upon pyruvate kinase simulations, preformed elsewhere (Naithani et al. 2015). Specifically, the simulation used a 1.0-Å hydrated cubic environment, all force fields and a neutral environment with 12 sodium ions at 25 °C for 10 ns.

Analytical ultracentrifugation

Analytical ultracentrifugation studies were performed in a Beckman model XL-I analytical ultracentrifuge with conventional double-sector charcoal-epon centrepieces with quartz windows in a four-hole An60-Ti rotor at 20 °C. An absorbance optical system was used at a wavelength of 280 nm. Solvent density (1.005 g/mL), solvent viscosity (0.0102 poise) and an estimate of the partial specific volume (0.7392) for PK[TIM+Reg] were computed using SEDNTERP (Laue et al. 2007).

For sedimentation velocity experiments, 400 μL of reference buffer (20 mM Tris-HCl and 150 mM NaCl, pH 8) and 380 μL of sample (1 mg/mL PK$^{TIM+Reg}$ in reference buffer) were centrifuged at 50,000 rpm. Data were collected at a single wavelength at 6 min intervals using a 0.003 cm step size in continuous mode. Sedimentation velocity data at multiple time points were fitted to a continuous size distribution $c(s)$ model using SEDFIT and regularized with the maximum entropy method (set at 0.95), standard for continuous distribution model fitting (Schuck et al. 2002). For sedimentation equilibrium experiments, reference and sample sectors were loaded with 120 μL of reference buffer and 100 μL of protein sample, respectively. Samples were centrifuged at 8,000 and 11,500 rpm, with the two speeds used to ensure that the resulting data is sufficiently to estimate the mass of an ~200 kDa protein. Data were collected every 4 h until sedimentation equilibrium was attained, at 280 nm, using a 0.001 cm step size in step mode and an average of 10 measurements. Sedimentation equilibrium and velocity data were globally fitted to a to a single discrete species with mass conservation model using SEDPHAT (Vistica et al. 2004). Theoretical sedimentation coefficient for the molecular dynamics model and wild-type crystal structure (PDB: 4YNG) using HYDROPRO (Ortega et al. 2011). The models were analysed at the residue level with a 4.8 Å shell calculation and simulating the experimental conditions, all other options were automated.

Small-angle X-ray scattering and *ab initio* model building

Small-angle X-ray scattering (SAXS) data were collected at the Australian Synchrotron (Melbourne, Australis) on the SAXS/WAXS beamline. The X-ray beam size at the sample was 250 μm horizontal and 80 μm vertical, and data were collected using a Pilatus 1M detector positioned 900 mm from the sample, giving a q-range of 0.01–0.6 Å^{-1} (wavelength, 1.0332 Å). The protein sample was subjected to in-line size exclusion chromatography on a Superdex 200 5/150 GL gel filtration column (GE Healthcare) equilibrated with buffer. The PK$^{TIM+Reg}$ (50 μl, 12 mg/mL) fractionated sample was passed through a 1.5-mm quartz capillary, where it was exposed to the X-ray beam. A total of 600 detector images, consisting of sequential 5-s exposures, were collected. Averaged background buffer scattering was subtracted from the peak scattering using Scatterbrain (version 2.82). Scattering error was halved, as Scatterbrain outputs at twice the value of the standard error (Trewhella et al. 2017). Guinier plots were analysed using SAS ATSAS data analysis software package (version 2.8) (Franke et al. 2017) and P(r) distribution analysis was performed using GNOM (Svergun 1992). Theoretical scattering curves were generated from atomic coordinates and compared with experimental scattering curves using CRYSOL (Svergun et al. 1995). DAMMIF was

used to generate bead models that fit the scattering pattern of the experimental data, selecting a tetramer with P222 symmetry (Franke and Svergun 2009). The DAMAVER suite of software was used to average 20 of the bead models to generate the most probable model (Volkov and Svergun 2003). SUPCOMB was then used to superimpose the 3D bead model onto the crystal structures (Kozin and Svergun 2001). Finally, GASBOR was used to produce 10 chain-like ensemble bead models, selecting P222 symmetry, reciprocal space fit and 373 dummy residues options (Petoukhov and Svergun 2003).

Results and Discussion

Engineering and purifying a recombinant, lidless pyruvate kinase

To examine the role of the lid domain and to assess whether it is essential for catalytic function, a pyruvate kinase variant was engineered without a lid domain (PK$^{TIM+Reg}$). We did this by engineering the gene such that the lid domain (residues 71-170) was removed and replaced with a hairpin loop to link residues 70 and 171, which required a mutational change from P70 to A70. This strategy was chosen because in the wild-type structure, the lid domain is installed in a C-terminal loop of the TIM barrel between β-strand 3 and α-helix 3 (PDB:4YNG), and the residues that attach the lid domain are in close proximity (5.9 Å) (**Fig. 1a**).

[INSERT FIGURE 1]

Soluble expression and purification of PK$^{TIM+Reg}$ was assessed using SDS-PAGE. Based on the amino acid sequence of the PK$^{TIM+Reg}$ construct, the protein was estimated have a monomeric mass of 42.8 kDa. In line with this estimate, a large band consistent with PK$^{TIM+Reg}$ overexpression was visible at approximately 43 kDa. Both chromatography steps increased protein purity and the final sample was estimated to be >95% pure (**Fig. 1b**). That the protein was easily overexpressed and purified suggests that removal of the lid domain does not significantly destabilise the protein. Importantly, using immobilised nickel affinity strategy for purification negated the possibility of co-purifying endogenous wild-type enzyme, which would confound the kinetic results.

PK$^{TIM+Reg}$ is catalytically active

Next, we examined whether removal of the lid domain affected the catalytic function of the protein using a lactate dehydrogenase coupled assay. We found that the recombinant PK$^{TIM+Reg}$ enzyme is catalytically active, with a measurable decrease in 340 nm absorbance demonstrating that NADH was consumed in the coupled assay. To confirm that the catalytic activity measured was due to PK$^{TIM+Reg}$, rather than endogenous pyruvate kinase from the expression strain, the protein expression and purification steps described above were repeated using a control *E. coli* strain containing only the empty pET-28b+ vector and catalytic activity measured. There was no enzymatic activity measured in any of the bound fractions, suggesting that the PK$^{TIM+Reg}$ enzyme is the only catalytically active species in the sample.

The kinetic parameters of PK$^{TIM+Reg}$ were then determined by collecting initial rate data against increasing substrate concentration. Initial rates were dependent on the concentrations of both substrates, adenosine diphosphate and phosphoenolpyruvate, confirming that pyruvate (used in the coupled assay) is produced and that both substrates are used by PK$^{TIM+Reg}$. The initial rate data versus increasing adenosine diphosphate concentration was fitted to a Michaelis-Menten kinetic model that gave an apparent $K_M^{adenosine\ diphosphate}$ of 1.0 ± 0.2 mM (**Fig. 2**). The data for increasing phosphoenolpyruvate concentration was fitted to an allosteric sigmoidal model that gave an apparent $S_{0.5}^{phosphoenolpyruvate}$ of 0.33 ± 0.01 mM (**Fig. 2**). The apparent $K_M^{adenosine\ diphosphate}$ is unchanged relative to the wild-type enzyme ($K_M^{adenosine\ diphosphate}$ = 1.0 ± 0.1 mM (Zhu et al. 2010)), but the apparent $S_{0.5}^{phosphoenolpyruvate}$ is significantly different ($S_{0.5}^{phosphoenolpyruvate}$ = 0.06 ±0.002 mM (Zhu et al. 2010)), which further demonstrates that the activity measured is not from endogenously purified pyruvate kinase. The values are generally similar to those of other characterised pyruvate kinases, for which $K_M^{adenosine\ diphosphate}$ values ranging from 0.03–2.3 mM and $S_{0.5}^{phosphoenolpyruvate}$ values ranging from 0.02–1.2 mM have been reported (Feksa et al. 2004; Oria-Hernández et al. 2005; Pizzuto et al. 2010; Saito et al. 2008; Susan-Resiga and Nowak 2004). The k_{cat} value for PK$^{TIM+Reg}$ was 0.0031 ±0.0004 min^{-1}, which is 10^6–10^8-fold lower than the k_{cat} values reported for other characterised pyruvate kinases (range, 2,800–71,000 min^{-1}) (Feksa et al. 2004; Oria-Hernández et al. 2005; Pizzuto et al. 2010; Saito et al. 2008; Susan-Resiga and Nowak 2004). Therefore, we have shown that while PK$^{TIM+Reg}$ can bind both substrates effectively, the absence of the lid region attenuates the catalytic function of the enzyme.

      [INSERT FIGURE 2]

We next compared the values obtained in the current study with pyruvate kinase variants investigated in previous studies aimed at defining the catalytic mechanism. In the lid domain (residues 71–170), D127 and E71 (*E. coli* numbering) have been implicated in the catalytic process (Morgan et al. 2010). For pyruvate kinase from *Leishmania mexicana*, the residue equivalent to D127 coordinates Mg^{2+}, which binds to adenosine diphosphate when the lid is closed for catalysis (Morgan et al. 2010) (**Fig. S1**). Coordination between D127 and Mg^{2+} is likely to increase the nucleophilicity of adenosine diphosphate to enhance the phosphate transfer from phosphoenolpyruvate. Additionally, the residue corresponding to E71 in *L. mexicana* pyruvate kinase was shown to interact with K$^+$, which in turn interacts with Mg^{2+} and phosphoenolpyruvate (Morgan et al. 2010) (**Fig. S1**). Interestingly, the residue at this position tends to be a glutamate in K$^+$-dependent pyruvate kinases, including those from *E. coli*, while a lysine residue is usually found

in K^{+}-independent pyruvate kinases (Oria-Hernández et al. 2005; Oria-Hernández et al. 2006). Substitution experiments in the K^{+}-dependent human pyruvate kinase demonstrated that changing the glutamate to lysine facilitates K^{+}-independent catalysis (Oria-Hernández et al. 2005). However, the resulting substituted enzyme had a lower k_{cat} value than the wild-type K^{+}-dependent enzyme (9,600 min^{-1} vs. 71,000 min^{-1}) and a slightly increased $K_M^{phosphoenolpyruvate}$ (0.13 mM vs. 0.24 mM) (Oria-Hernández et al. 2005). Together, these comparisons demonstrate that D127 is important for catalysis, and that E71 is important for catalysis and phosphoenolpyruvate association. Therefore, absence of both residues could largely be responsible for the decreased catalytic function of PK$^{TIM+Reg}$.

Our kinetic studies also demonstrate that the allosteric features of pyruvate kinase are altered by removing the lid domain. Firstly, in the absence of fructose-1,6-bisphosphate, no activity is observable. This confirms that PK$^{TIM+Reg}$ retains allosteric activation by fructose-1,6-bisphosphate, which is expected since the activator binds at the regulatory domain of PK$^{TIM+Reg}$ distal from the removed lid domain. Secondly, in the presence of the allosteric activator fructose-1,6-bisphosphate (2 mM), PK$^{TIM+Reg}$ is cooperatively activated by the substrate phosphoenolpyruvate (n_H = 1.7), whereas for the wild-type enzyme n_H = 1.0 (Valentini et al. 2000). *E. coli* pyruvate kinase is proposed to follow a 'rock and lock' model for allosteric activation, where fructose-1,6-bisphosphate binding locks the enzyme into the activated R-state (Donovan et al. 2016b; Morgan et al. 2010). The R-state conformation is thought to be locked into this active R-state through the interaction of D127 from the lid domain and R292 from the opposing subunit (Mattevi et al. 1995). Therefore, destabilisation of the R-state of PK$^{TIM+Reg}$ is expected to be consistent with the absence of the lid domain, and the utilisation of the rock and lock model for allosteric activation for *E. coli* pyruvate kinase.

In summary, PK$^{TIM+Reg}$ is considerably less active than the wild-type enzyme, although it is still able to catalyse the reaction. Removing the lid domain also increases the $S_{0.5}$ for phosphoenolpyruvate, but has little effect on the K_M for adenosine diphosphate, consistent with the known catalytic roles of residues in the lid domain. Moreover, the regulation profile of the enzyme is subtly altered: PK$^{TIM+Reg}$ retains allosteric activation by fructose-1,6-bisphosphate, but is co-operatively activated by phosphoenolpyruvate even in the presence of fructose-1,6-bisphosphate, unlike the wild-type enzyme.

The PK$^{TIM+Reg}$ structure retains a tetrameric configuration

To assess whether the removal of the lid domain has compromised catalytic activity through destabilisation of the structure, we performed thermal denaturation studies of PK$^{TIM+Reg}$ and determined its solution structure. The thermal stability profiles of PK$^{TIM+Reg}$ and the wild-type enzyme revealed an 11 °C decrease in unfolding temperature (**Fig. S2a, b**) and indicates that absence of the lid domain has destabilised the protein. The reasons for the observed decrease in melting temperature is not immediately apparent. The wild-type enzyme is larger, which could be a factor that increases stability, but as the lid region is not part of the protein core and compactness is thought to be a leading factor influencing melting temperature (Kumar et al. 2000), size alone is not thought to explain the lower thermal stability of PK$^{TIM+Reg}$. Potentially, the lower melting point may reflect that the engineered hairpin loop is not ideal, as compared to the wild-type lid linker region, and PK$^{TIM+Reg}$ is missing a coevolved property that stabilises the TIM barrel. Loss of stabilisation could contribute to the decreased catalytic function of the mutant enzyme.

The thermal denaturation assay was also used to investigate binding of fructose-1,6-bisphosphate, which is responsible for the allosteric activation of pyruvate kinase by binding in the regulatory domain (residues 352–470) (Mattevi et al. 1995). This was of interest because while the kinetic data demonstrates that fructose-1,6-bisphosphate is an activator of PK$^{TIM+Reg}$ catalytic activity, but it does not completely stabilise the R-state (n_H = 1.7), and is different than wild-type enzyme (n_H = 1.0) (Valentini et al. 2000). In the thermal shift assay, addition of fructose-1,6-bisphosphate decreased the melting temperature of wild-type pyruvate kinase from 59 °C to 56 °C (**Fig. S2a**), with a similar decrease in melting temperature observed for PK$^{TIM+Reg}$ (48 °C to 44 °C) (**Fig. S2b**). This similarity, alongside the kinetic data, suggests that the regulatory domain of PK$^{TIM+Reg}$ is correctly folded to facilitate binding of fructose-1,6-bisphosphate and interaction is likely to be similar.

Wild type pyruvate kinase has a tetrameric configuration, which is known to be important for catalysis and allosteric regulation (Mattevi et al. 1995). To investigate the oligomeric properties of PK$^{TIM+Reg}$ analytical ultracentrifugation sedimentation experiments were conducted. Sedimentation velocity scan data presents with a steep absorbance boundary that is consistent with the sample containing a single dominant species (**Fig. 3a**). When fitted to a c(s) model, as implemented in SEDFIT (Schuck 2000), there is a main peak (92% of absorbance signal) at 7.1 S and a short distributed peak (5% of absorbance signal) at approximately 11 S (**Fig. S3**). The mass of the components was then examined SEDPHAT using species analysis with mass conservation

constraints (Vistica et al. 2004) with global fitting of the velocity and equilibrium data (**Fig. 3b**). The buoyant mass of the 7.1 S molecule was determined to be 170.4 kDa, which closely matches the calculated tetrameric mass (171.2 kDa), indicating that the PK$^{TIM+Reg}$ is a tetramer. The 11 S component was over 1.3 kDa, which is likely to be some aggregate as no large components were visible on the SDS PAGE gel. No monomeric or dimeric species were observed indicating that the main oligomeric state is stable as a tetramer, which is consistent with the solution structure of wild-type pyruvate kinase (Zhu et al. 2010). Retention of the tetrameric form suggests that the tetrameric interfaces at both the TIM catalytic domain and the C-terminal regulatory domain remain intact, and that PK$^{TIM+Reg}$ folds similarly to the wild-type.

[INSERT FIGURE 3]

Analytical ultracentrifugation data was compared with structural data to investigate the potential size and shape of PK$^{TIM+Reg}$. The sequence of PK$^{TIM+Reg}$ is 77 aa shorter and the tetrameric mass is expected to be 31.7 kDa lower than wild type pyruvate kinase (171.2 vs. 202.9 kDa). The sedimentation experiments for PK$^{TIM+Reg}$ (above), and for the previously tested wild type enzyme (Zhu et al. 2010), are consistent with these masses. The sedimentation coefficients have a similar difference, PK$^{TIM+Reg}$ 7.1 S vs. wild type 8.5 S (Zhu et al. 2010), with the coefficient value of globular proteins largely influenced by the difference in particle mass (Laue and Stafford III 1999). A molecular dynamic simulated structure of PK$^{TIM+Reg}$ based upon the wild type tetrameric configuration and the wild type crystal structure were used to model the sedimentation coefficients with HYDROPRO (Ortega et al. 2011). The modelled sedimentation coefficient for PK$^{TIM+Reg}$ is 7.5 S, and the wild type value is 8.5 S, which are both close to the corresponding experimental values (7.1 and 8.5 S). Therefore, the overall size and shape of PK$^{TIM+Reg}$ is largely consistent with the wild-type tetrameric structural configuration, except for the absence of the lid domain.

Small-angle X-ray scattering was then used to investigate the solution structure of PK$^{TIM+Reg}$. The Guiner plot was linear, indicating that the sample was clear of aggregates and interparticle interference (**Fig. 4a**, inset). Analysis of the scatter calculated D_{max} at 129 Å and R_g at 41.5 Å. A homology model was then built and solvated using molecular dynamic simulations for comparison with the small-angle X-ray scattering data. The final model for PK$^{TIM+Reg}$ resembles the wild-type template, but without the lid domain. Analysis of the structure by HullRad (Fleming and Fleming 2018) revealed a D_{max} of 126 Å and anhydrous R_g of 39.8 Å, which is consistent with the solvated

experimental values (D_{max} of 129 Å and R_g of 41.5 Å). This demonstrates that PK$^{TIM+Reg}$ is the same size as the wild-type enzyme structure with the lid domain removed.

[INSERT FIGURE 4]

The wild-type pyruvate kinase tetramer assembles as a dimer of dimers, with the dimers formed through an association between the TIM barrel domains and the final tetramer formed via association of the regulatory domains (Donovan et al. 2016a). To investigate the oligomeric form of PK$^{TIM+Reg}$, we first compared the experimental scatter with the theoretical scatter of PK$^{TIM+Reg}$ models. Theoretical scatter for the wild-type pyruvate kinase, the homology model and the molecular dynamics-simulated model was overlaid with the scattering data (**Fig. 4a**). For the wild-type enzyme, the theoretical scatter sits above the scattering data for PK$^{TIM+Reg}$ at the low q range, which is consistent with the wild-type enzyme being larger, and at the mid-ranges (0.5-0.2 Å^{-1}) the wild-type has a pattern that is more linear, which is consistent with the expectation that the wild-type enzyme is more asymmetric than PK$^{TIM+Reg}$ (**Fig. 4b**) (Mertens and Svergun 2010). Examination of the PK$^{TIM+Reg}$ molecular dynamics model theoretical scatter in the same ranges reveals no significant divergence in the low and mid-ranges, indicating that the molecular dynamics model is a good fit for the size and shape of PK$^{TIM+Reg}$. Quantitative comparison of the theoretical scatter with the experimental data revealed χ^2 values of 25.3 for the wild-type protein, 5.8 for the homology model, and 1.1 for the model that had been relaxed using molecular dynamics simulations. This confirms that the solution scatter of PK$^{TIM+Reg}$ strongly correlates with the constructed homology model, which was subsequently improved through molecular dynamic simulations

To further investigate the oligomeric form of PK$^{TIM+Reg}$, *ab initio* bead models were constructed from the experimental scattering data. As previously discussed, the molecular dynamics model is likely to provide a representation of the size and shape of PK$^{TIM+Reg}$, but as the simulation uses the wild-type structure as a template it can be biased. *Ab initio* modelling using the experimental data was therefore used to provide a model that was not predisposed to the wild-type configuration. First, models were constructed using P1 symmetry, this gave low χ^2 values indicating good correlation with the experimental scatter but had shapes that did not appear to be built using four monomeric subunits and was unlikely to be representative of the PK$^{TIM+Reg}$ tetramer. P2 and P222 symmetry options were then trialled, P222 had lower χ^2 values indicating it was more representative and was used for subsequent model building. Class-averaged models were produced by DAMMIF and DAMAVER (Petoukhov and Svergun 2003) and have an oblate twisted

octagonal discoid shape that neatly fits the volume of the PK$^{TIM+Reg}$ molecular dynamics model (**Fig. 4c**). Ten single models were constructed using Gasbor to produce a high-resolution model from the small-angle X-ray scattering data, then each was rated for correlation with the experimental data based on χ^2 values using CRYSOL (Svergun et al. 1995). The best model (χ^2 = 1.3) had a twisted oblate shape with no central density, and closely matched the PK$^{TIM+Reg}$ molecular dynamics model when overlaid (**Fig. 4d**). Combined, the comparisons show that the solution structure of PK$^{TIM+Reg}$ is similar to the molecular dynamics model that is assembled from a dimer of dimers with a hole at the centre, and therefore highly consistent with the wild-type formation.

In conclusion, the solution structural studies demonstrate that PK$^{TIM+Reg}$ forms a tetramer in a manner consistent with the wild-type pyruvate kinase and that the TIM and regulatory are likely to be assembled correctly. Therefore, PK$^{TIM+Reg}$ forms a stable structure, which is not materially destabilised by the absence of the lid domain. We conclude that PK$^{TIM+Reg}$ is structurally representative of pyruvate kinase without a lid and its absence is the significant factor for decreased catalytic activity.

Conclusions

Engineering a lidless pyruvate kinase allowed us to assess the essentiality of the lid domain in catalysis. Surprisingly, despite previous studies showing that the lid domain contributes key residues to the catalytic site, PK[TIM+Reg] is able to bind the substrates, phosphoenolpyruvate and adenosine diphosphate, although the phosphoenolpyruvate affinity is decreased compared to the wild-type enzyme, and is catalytically functional, albeit severely attenuated. Thus, data presented in this study demonstrate that the lid domain is not *essential* for catalytic function but is *necessary* for efficient catalysis.

The lid domain is highly conserved in pyruvate kinase enzymes, which suggests it plays a key functional role. Our data is consistent with the lid domain executing a catalytic role, which is proposed elsewhere (Morgan et al. 2010; Oria-Hernández et al. 2005). The lower catalytic rate and decreased phosphoenolpyruvate affinity are consistent with the loss of residue E71 at the lid hinge region, where this residue has a role in active site K^+ binding (Morgan et al. 2010; Oria-Hernández et al. 2005). Reduction of the catalytic rate is also consistent with loss of D127 that coordinates to active site Mg^{2+} (Morgan et al. 2010). The lid domain also has a role in regulation, and stabilises the activated R-state that is induced by fructose-1,6-bisphosphate binding (Valentini et al. 2000). Our results are consistent with this role, as the R-state was not fully stabilised in PK[TIM+Reg] without phosphoenolpyruvate (n_H 1.7 vs. wild-type, n_H = 1.0). Additionally, the lid may play a substantial role in cooperative upregulation through phosphoenolpyruvate binding. The rationale for this is that wild-type pyruvate kinase is cooperatively upregulated by phosphoenolpyruvate binding when fructose-1,6-bisphosphate is absent and maximum catalytic rates are only slightly reduced compared to when fructose-1,6-bisphosphate is present. In contrast, PK[TIM+Reg] catalytic rates were not observable when fructose-1,6-bisphosphate is absent. Therefore, we tentatively suggest that activation by cooperative phosphoenolpyruvate binding occurs similarly to allosteric activation by fructose-1,6-bisphosphate, but in reverse. Specifically, substrate binding causes the lid domain to close and places D127 near R272 from the opposing subunit (as demonstrated by the oxaloacetate and ATP bound *L.* Mexicana structure, PDB: 3HQO), which subsequently unlocks the R-state and initiates the reciprocal rotation at the regulatory domain.

Our data reveals that removing the lid domain does not alter the folding of the protein or the formation of the tetrameric structure. Thermal shift assays demonstrate that the presence of fructose-1,6-bisphospate decreases the melting temperature of both the wild-type and PK[TIM+Reg],

which is consistent with the binding of fructose-1,6-bisphosphate inducing an increase in dynamic motion, as previously described (Donovan et al. 2016b). Even without the lid domain, analytical ultracentrifugation studies show that PK$^{TIM+Reg}$ forms as a tetramer and small-angle X-ray scattering indicates that the structure is highly likely to be an oblate twisted ring, very similar to that of the wild-type enzyme. The lid domain is therefore not essential for fructose-1,6-bisphosphate induced activation or formation of the oligomeric assembly. Therefore, we propose the differences in catalytic function cannot be attributed to structural destabilisation and reflect the engineering of the lidless enzyme.

Our study allows us to speculate on an evolutionary trajectory that led to the efficient pyruvate kinase structure. We propose that a lidless ancestor enzyme had low pyruvate kinase activity, and this was perhaps a moonlighting function of the ancestor enzyme. Insertion of the lid domain within a C-terminal loop of the TIM barrel domain increased the catalytic activity of the enzyme and was subsequently selected for by natural selection, as increased activity would allow increased flux through the glycolytic pathway, providing the cell an advantage when utilising carbohydrates as a primary energy source.

Overall, this study sheds light on the catalytic function of pyruvate kinase and provides data that may be of use to others seeking to engineer pyruvate kinases to manipulate metabolism in cellular engineering, or for those seeking inhibitors of pyruvate kinase in clinical settings.

Acknowledgements

Declarations

Conflicts of interest: none

Availability of data and material: On request.

Code availability: N/A

Authors' contributions: ES, KAD, and RCJD conceived the project. ES conducted the experiments. ES, DW, and DC analysed and interpreted the data. RCJD secured funding for the work. ES, DW, and DC drafted the manuscript. All authors read and edited the manuscript.

References

Abraham MJ, Murtola T, Schulz R, Páll S, Smith JC, Hess B, Lindahl E (2015) GROMACS: High performance molecular simulations through multi-level parallelism from laptops to supercomputers. SoftwareX 1:19-25

Ainscow EK, Brand MD (1999) Top-down control analysis of ATP turnover, glycolysis and oxidative phosphorylation in rat hepatocytes. Eur J Biochem 263:671-685

Arnold K, Bordoli L, Kopp J, Schwede T (2006) The SWISS-MODEL workspace: a web-based environment for protein structure homology modelling. Bioinformatics 22:195-201

Donovan KA, Atkinson SC, Kessans SA, Peng F, Cooper TF, Griffin MD, Jameson GB, Dobson RC (2016a) Grappling with anisotropic data, pseudo-merohedral twinning and pseudo-translational noncrystallographic symmetry: a case study involving pyruvate kinase. Acta Crystallogr, Sect D: Struct Biol 72:512-519

Donovan KA, Zhu S, Liuni P, Peng F, Kessans SA, Wilson DJ, Dobson RCJ (2016b) Conformational dynamics and allostery in pyruvate kinase. J Biol Chem 291:9244-9256

Emsley P, Lohkamp B, Scott WG, Cowtan K (2010) Features and development of Coot. Acta Crystallogr, Sect D: Struct Biol 66:486-501

Feksa LR, Cornelio A, Dutra-Filho CS, de Souza Wyse AT, Wajner M, Wannmacher CMD (2004) Inhibition of pyruvate kinase activity by cystine in brain cortex of rats. Brain Res 1012:93-100

Fenton AW, Reinhart GD (2002) Isolation of a single activating allosteric interaction in phosphofructokinase from *Escherichia coli*. Biochemistry 41:13410-13416

Fleming PJ, Fleming KG (2018) HullRad: fast calculations of folded and disordered protein and nucleic acid hydrodynamic properties. Biophys J 114:856-869

Franke D, Petoukhov M, Konarev P, Panjkovich A, Tuukkanen A, Mertens H, Kikhney A, Hajizadeh N, Franklin J, Jeffries C (2017) ATSAS 2.8: a comprehensive data analysis suite for small-angle scattering from macromolecular solutions. J Appl Crystallogr 50:1212-1225

Franke D, Svergun DI (2009) DAMMIF, a program for rapid ab-initio shape determination in small-angle scattering. J Appl Crystallogr 42:342-346

Johnsen U, Hansen T, Schönheit P (2003) Comparative analysis of pyruvate kinases from the hyperthermophilic archaea *Archaeoglobus fulgidus*, *Aeropyrum pernix*, and *Pyrobaculum aerophilum* and the hyperthermophilic bacterium *Thermotoga maritima.* Unusual regulatory properties in hyperthermophilic archaea. J Biol Chem 278:25417-25427

Kozin MB, Svergun DI (2001) Automated matching of high-and low-resolution structural models. J Appl Crystallogr 34:33-41

Kumar S, Tsai C-J, Nussinov R (2000) Factors enhancing protein thermostability. Protein Eng, Des Sel 13:179-191

Laue T, Shah B, Ridgeway T, Pelletier S (2007) SEDNTERP. Anal Ultracentrifugation Biochem Polym Sci 90125

Laue T, Stafford III W (1999) Modern applications of analytical ultracentrifugation. Annu Rev Biophys Biomol Struct 28:75-100

Li F, Yu T, Zhao Y, Yu S (2012) Probing the catalytic allosteric mechanism of rabbit muscle pyruvate kinase by tryptophan fluorescence quenching. Eur Biophys J 41:607-614

Malcovati M, Valentini G (1982) AMP-and fructose 1, 6-bisphosphate-activated pyruvate kinases from Escherichia coli Methods Enzymol, vol 90. Elsevier, pp 170-179

Mattevi A, Bolognesi M, Valentini G (1996) The allosteric regulation of pyruvate kinase. FEBS Lett 389:15-19

Mattevi A, Valentini G, Rizzi M, Speranza ML, Bolognesi M, Coda A (1995) Crystal structure of *Escherichia coli* pyruvate kinase type I: molecular basis of the allosteric transition. Structure 3:729-741

Mertens HD, Svergun DI (2010) Structural characterization of proteins and complexes using small-angle X-ray solution scattering. Journal of structural biology 172:128-141

Morgan HP, McNae IW, Nowicki MW, Hannaert V, Michels PAM, Fothergill-Gilmore LA, Walkinshaw MD (2010) Allosteric mechanism of pyruvate kinase from *Leishmania mexicana* uses a rock and lock model. J Biol Chem 285:12892-12898

Nagano N, Orengo CA, Thornton JM (2002) One fold with many functions: the evolutionary relationships between TIM barrel families based on their sequences, structures and functions. J Mol Biol 321:741-765

Naithani A, Taylor P, Erman B, Walkinshaw MD (2015) A molecular dynamics study of allosteric transitions in *Leishmania mexicana* pyruvate kinase. Biophys J 109:1149-1156

Niesen FH, Berglund H, Vedadi M (2007) The use of differential scanning fluorimetry to detect ligand interactions that promote protein stability. Nature protocols 2:2212

Oria-Hernández J, Cabrera N, Pérez-Montfort R, Ramírez-Silva L (2005) Pyruvate kinase revisited: The activating effect of K^+. J Biol Chem 280:37924-37929

Oria-Hernández J, Riveros-Rosas H, Ramírez-Sílva L (2006) Dichotomic phylogenetic tree of the pyruvate kinase family: K^+-dependent and -independent enzymes. J Biol Chem 281:30717-30724

Ortega A, Amorós D, García de la Torre J (2011) Prediction of hydrodynamic and other solution properties of rigid proteins from atomic- and residue-level models. Biophys J 101:892-898

Pearce AK, Crimmins K, Groussac E, Hewlins MJ, Dickinson JR, Francois J, Booth IR, Brown AJ (2001) Pyruvate kinase (Pyk1) levels influence both the rate and direction of carbon flux in yeast under fermentative conditions. Microbiology 147:391-401

Pendergrass DC, Williams R, Blair JB, Fenton AW (2006) Mining for allosteric information: natural mutations and positional sequence conservation in pyruvate kinase. IUBMB life 58:31-38

Petoukhov MV, Svergun DI (2003) New methods for domain structure determination of proteins from solution scattering data. J Appl Crystallogr 36:540-544

Pizzuto R, Paventi G, Atlante A, Passarella S (2010) Pyruvate kinase in pig liver mitochondria. Arch Biochem Biophys 495:42-48

Reeves RE, Sols A (1973) Regulation of *Escherichia coli* phosphofructokinase in situ. Biochem Biophys Res Commun 50:459-466

Saito T, Nishi M, Lim MI, Wu B, Maeda T, Hashimoto H, Takeuchi T, Roos DS, Asai T (2008) A novel GDP-dependent pyruvate kinase isozyme from *Toxoplasma gondii l*ocalizes to both the apicoplast and the mitochondrion. J Biol Chem 283:14041-14052

Schormann N, Hayden KL, Lee P, Banerjee S, Chattopadhyay D (2019) An overview of structure, function, and regulation of pyruvate kinases. Protein Sci 28:1771-1784

Schuck P (2000) Size-distribution analysis of macromolecules by sedimentation velocity ultracentrifugation and lamm equation modeling. Biophys J 78:1606-1619

Schuck P, Perugini MA, Gonzales NR, Howlett GJ, Schubert D (2002) Size-distribution analysis of proteins by analytical ultracentrifugation: strategies and application to model systems. Biophys J 82:1096-1111

Sterner R, Höcker B (2005) Catalytic versatility, stability, and evolution of the (βα) 8-barrel enzyme fold. Chem Rev 105:4038-4055

Susan-Resiga D, Nowak T (2004) Proton donor in yeast pyruvate kinase: Chemical and kinetic properties of the active site Thr 298 to Cys mutant. Biochemistry 43:15230-15245

Svergun D (1992) Determination of the regularization parameter in indirect-transform methods using perceptual criteria. J Appl Crystallogr 25:495-503

Svergun D, Barberato C, Koch MH (1995) CRYSOL–a program to evaluate X-ray solution scattering of biological macromolecules from atomic coordinates. J Appl Crystallogr 28:768-773

Trewhella J, Duff AP, Durand D, Gabel F, Guss JM, Hendrickson WA, Hura GL, Jacques DA, Kirby NM, Kwan AH (2017) 2017 publication guidelines for structural modelling of small-angle scattering data from biomolecules in solution: an update. Acta Crystallogr, Sect D: Struct Biol 73:710-728

Valentini G, Chiarelli L, Fortin R, Speranza ML, Galizzi A, Mattevi A (2000) The allosteric regulation of pyruvate kinase A site-directed mutagenesis study. J Biol Chem 275:18145-18152

Valentini G, Chiarelli LR, Fortin R, Dolzan M, Galizzi A, Abraham DJ, Wang C, Bianchi P, Zanella A, Mattevi A (2002) Structure and function of human erythrocyte pyruvate kinase. Molecular basis of nonspherocytic hemolytic anemia. J Biol Chem 277:23807-23814

Van Schaftingen E (1993) Glycolysis revisited. Diabetologia 36:581-588

van Wijk R, Huizinga EG, van Wesel AC, van Oirschot BA, A. Hadders M, van Solinge WW (2009) Fifteen novel mutations in PKLR associated with pyruvate kinase (PK) deficiency: structural implications of amino acid substitutions in PK. Hum Mutat 30:446-453

Vistica J, Dam J, Balbo A, Yikilmaz E, Mariuzza RA, Rouault TA, Schuck P (2004) Sedimentation equilibrium analysis of protein interactions with global implicit mass conservation constraints and systematic noise decomposition. Anal Biochem 326:234-256

Volkov VV, Svergun DI (2003) Uniqueness of *ab initio* shape determination in small-angle scattering. J Appl Crystallogr 36:860-864

Xie L, Wang DI (1996) Energy metabolism and ATP balance in animal cell cultivation using a stoichiometrically based reaction network. Biotechnol Bioeng 52:591-601

Zhu T, Bailey MF, Angley LM, Cooper TF, Dobson RC (2010) The quaternary structure of pyruvate kinase type 1 from *Escherichia coli* at low nanomolar concentrations. Biochimie 92:116-120
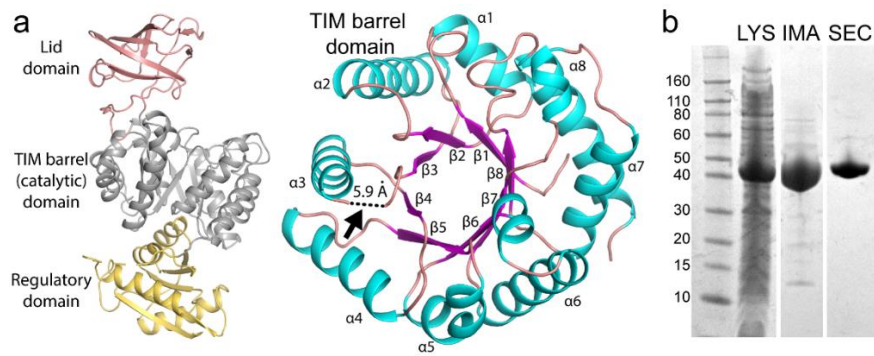
Fig. 1 Engineering and expression of PK[TIM+Reg]. **a** Pyruvate kinase has three domains: the catalytic TIM barrel, the small β-barrel lid domain and the C-terminal regulatory domain. The lid domain is formed as an outcrop from the edge of the TIM barrel domain. The anchor points of lid domain are separated by only 5.9 Å (arrow). TIM barrels are common stable structural elements with eight interlocking units of antiparallel α-helix and β-sheet domains (Nagano et al. 2002), which allowed the construction of PK[TIM+Reg] by removing the lid residues and replacing the section with a small hairpin loop. **b** Expression of PK[TIM+Reg]. SDS-PAGE gels showing overexpression of a protein within the cell lysate (LYS) at ~43 kDa, which matches the expected mass of PK[TIM+Reg]. Purification by immobilised metal affinity (IMA) and size exclusion chromatography (SEC) resulted in a final sample that was >95% pure
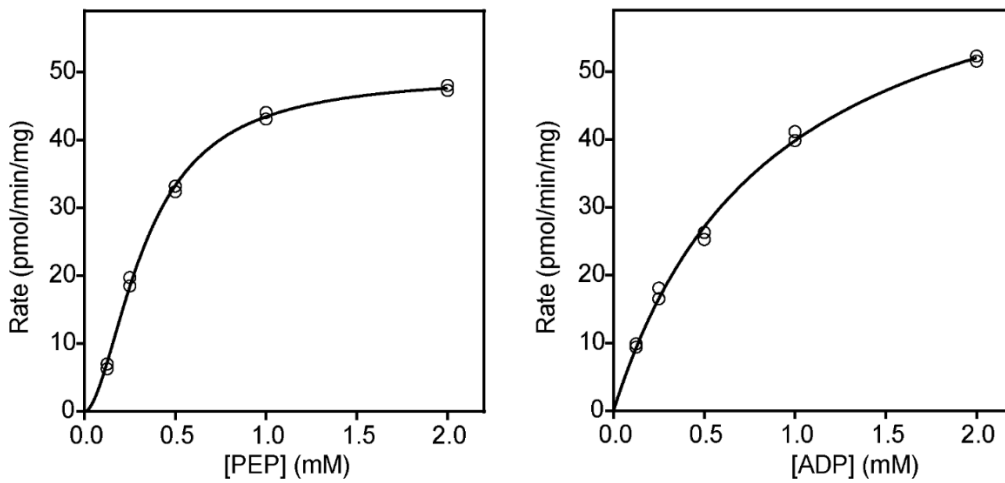
Fig. 2 Initial rate kinetics of PK$^{TIM+Reg}$. For phosphoenolpyruvate, the data was fit to an allosteric sigmoidal curve giving kinetic parameters; $S_{0.5}^{phosphoenolpyruvate}$ = 0.33 mM ± 0.01 and $n_H^{phosphoenolpyruvate}$ = 1.8 ± 0.1, which significantly different from the wild-type ($S_{0.5}^{phosphoenolpyruvate}$ = 0.08 mM and n_H = 1.0) (Valentini et al. 2000) and confirms that the activity measured is not from endogenously purified pyruvate kinase. For adenosine diphosphate, the data was fit to Michaelis-Menten curve giving kinetic parameters; $K_M^{adenosine\ diphosphate}$ = 1.0 ± 0.2 mM and k_{cat} = 0.0031 ± 0.0004 min^{-1}. The $K_M^{Adenosine\ diphosphate}$ is not significantly different, but the catalytic rate is severely compromised compared to the wild-type (10,000 min^{-1}) (Valentini et al. 2000; Zhu et al. 2010)
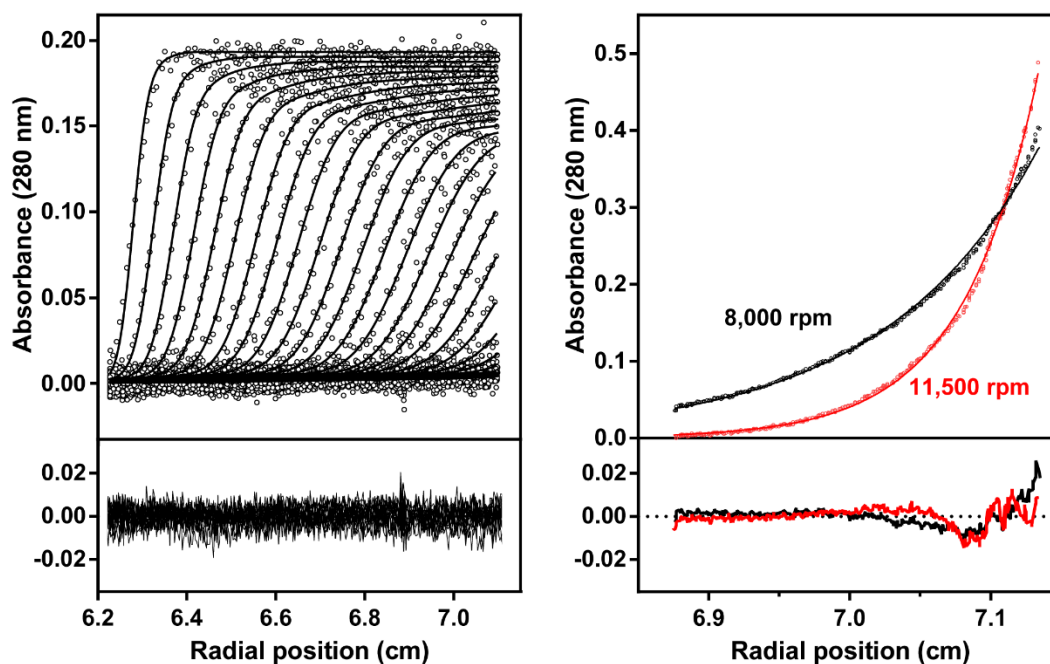
Fig. 3 Analytical ultracentrifugation data demonstrates that PK$^{TIM+Reg}$ retains it tetrameric state. Sedimentation velocity data (left) showing every second scan and third data point with baseline-subtracted and fitted for radial and time invariant noise. The profile shows a single step, steep absorbance boundary indicating that a single oligomeric species is dominate in the solution. The sedimentation velocity and sedimentation equilibrium scan data for PK$^{TIM+Reg}$ (right) were globally fit to a discrete species with mass conservation model, as implemented in SEDPHAT (Vistica et al. 2004). This gave a mass of 168.7 kDa, which closely corresponds with the predicted mass of the PK$^{TIM+Reg}$ tetramer mass (171 kDa). The global reduced χ^2 value for the fit was 0.21
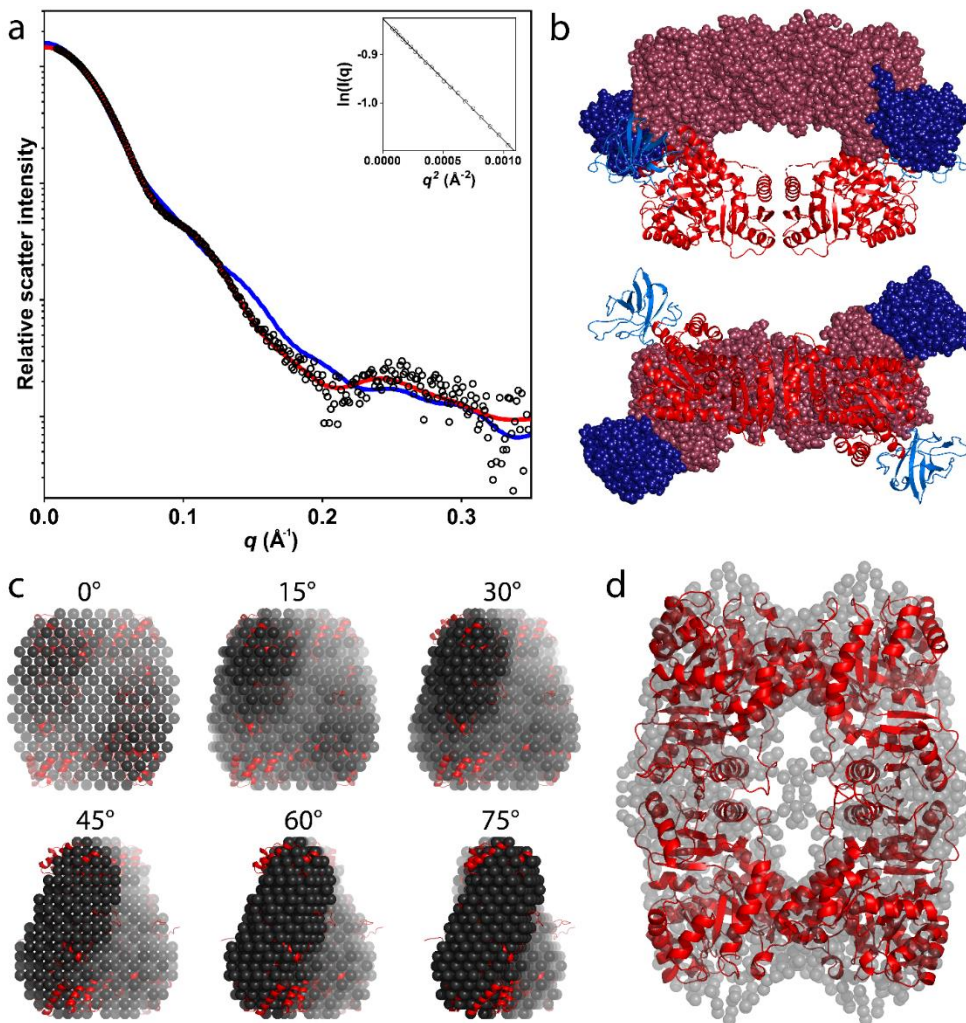
Fig. 4 Small-angle X-ray scattering and molecular dynamics models. **a** Small-angle X-ray scattering data (circles) compared with theoretical scatter of atomic models. Comparison with wild type pyruvate kinase reveals an χ^2 of 25.3 (blue), the PK$^{TIM+Reg}$ homology model has an χ^2 of 5.8 (not shown) and the final molecular dynamics model has an χ^2 of 1.1 (red), indicating that the molecular dynamics model is likely to resemble the true solution structure. Inset: Guinier plot of low-range data points revealed a linear trend, indicating a monodisperse solution suitable for molecular analysis. **b** Wild-type pyruvate kinase tetramer demonstrating the additional footprint of the lid domain (blue). Half the tetramer is shown as spheres to illustrate the oblate twist shape formed between the TIM and regulatory domains (red). **c** Group-averaged *ab initio* models produced using DAMMIF and DAMAVER match the PK$^{TIM+Reg}$ model and have the characteristic oblate twist shape (Franke and Svergun 2009; Volkov and Svergun 2003). **d** Single *ab initio* bead model of PK$^{TIM+Reg}$ produced using Gasbor ($\chi^2 = 1.3$) (Petoukhov and Svergun 2003). The bead model closely resembles the molecular dynamics model ($\chi^2 = 1.1$) and has a lack of density at the centre, as well as the oblate twist and profile expected for the engineered enzyme